Design, configuration, and thermal optimization of advanced cryostats

Quan-Sheng Shu[1], Jonathan Demko[2], James Fesmire[3], Robert Duckworth[4]

[1]Retired Scientist, Keller TX 76248 USA
[2]LeTourneau University, Longview, TX 75607 USA
[3]GenH2, Titusville, FL 32780, USA
[4]Oak Ridge National Laboratory, Oak Ridge, TN 37830 USA

Email: shu2012qs@hotmail.com

Abstract. To address new challenges in the design of current and future advanced cryostats, guidelines can be developed by leveraging successful technical experience with existing cryostat assemblies. A brief review of eleven representative advanced cryostat designs is presented, based on six typical cooling methods, including cryogen baths, dry cryostats, mixed-cooling method, continuous cryogen flow, dilution refrigeration, and demagnetization. Also provided are engineering figures, tables-plots, and equations that can be used to design, configure, and optimize the thermal performance of cryostats. The following technical data are introduced: optimal Carnot power versus temperature for various two heat intercept stations in cryostat support, ten representative performances of different MLI blankets at various (Th-Tc), and a graphical summary of the 'MLI patch-cover-crack' experiments, among others. The cold mass thermally isolated in cryostats could be a quantum apparatus, test specimen, instruments in-space, or superconducting (SC) devices. The cryostat must provide all functional interfaces for obtaining the required data. The design methodologies for crucial components of a cryostat are discussed in-depth, including: 1) creating a lightweight support structure and placing thermal anchors in optimal locations, 2) designing MLI systems with cost-effective thermal shields, and 3) constructing sophisticated structures to accommodate heavy RF couplers or current leads.

1. Introduction

Cryogenic applications rely on the availability of energy efficient cryostat assemblies, which have played a crucial role in a wide range of fields. The cryostat is a device designed to hold the cold mass (sample or apparatus) at cryogenic temperatures. It is isolated from the ambient environment by a vacuum chamber while providing all the necessary interfaces for reliable testing or performing special tasks. From the depths of the ocean to outer space and beyond, cryostats have enabled groundbreaking research, technological advances, and practical applications. Cryostats come in all shapes and sizes, ranging from palm-sized devices to massive superconducting accelerators and fusion Tokamaks, weighing hundreds of tons and spanning tens of kilometers. As extensively discussed in references [1-2], researchers are leveraging their extensive technical experience with existing cryostats to develop guidelines for addressing the challenges of further optimizing and expanding the use of these critical systems. A brief review of advanced cryostat designs currently in use is provided.

One effective approach for categorizing and summarizing developments in cryostat technology is based on their cooling methods. The cooling method is determined by the nature of the cold masses,

which in turn influences the design and performance of the cryostat. Design features are carefully selected to ensure efficient operation and desired functionality, particularly with respect to refrigeration requirements. In this paper, we present engineering figures, calculated table-plots, and representative equations for the design, configuration, and optimization of advanced cryostats in current and future applications. The following subjects are addressed in detail: 1) Examples of cryostats with different cooling methods; 2) Light-weight structure of cold mass supports and thermal anchors; 3) Designs of efficient MLI systems and intermediate T shields; and 4) Representative cryostats suitable for different applications with various cooling methods to demonstrate the integration of these technologies.

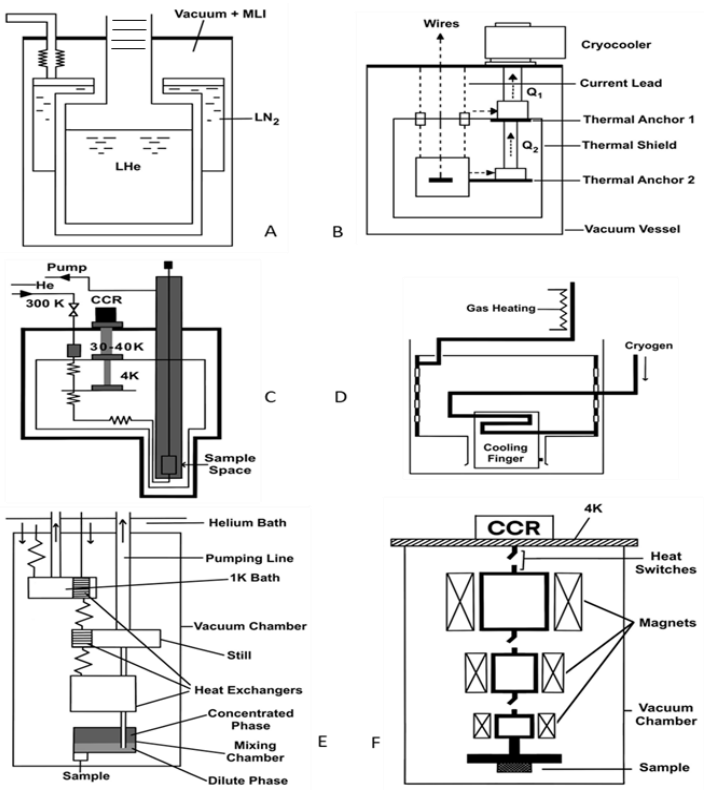

Figure 1. The main methods of cooling samples/apparatus in cryostats [1,3]: A – classic cryogen bath cryostat, B – dry cryostat (with cryocooler), C mixed-cooling cryostat, D – Cryostat with cryogen continuing flow, E – Cryostat cooled by dilution refrigerator, and F – Cryostat cooled by ADR.

2. Cooling Methods of Cryostats

The most crucial design issue is determining the appropriate cooling method, which is influenced by various criteria such as the required temperature and duration of cooling, the weight, volume, and geometry of the sample/apparatus, the working environment, and the cost. Successfully addressing these factors leads to the development of advanced and practical cryostats, as illustrated in Fig. 1[1,3].

2.1 Classic Cryostat Configuration

A classic cryostat (Fig. 1A) uses *cryogenic bath cooling* with LHe. Heat leaks are minimized using low thermal conductance support, MLI and LN2-cooled concentric thermal shields. Cryogens used depend on the required temperature: LHe for 1-4.2 K, LN2 for 63-78 K, and LH2 or solid H2 for ~20K. Advantages include stable temperature, minimal vibration, and low boil-off rates (~1%/hr), while disadvantages include the handling and storage of liquid cryogens.

The Figure 2A shows a classic cryostat made of stainless steel for laboratory testing, cooled by LHe bath with radiation baffles and a LN2 guard vessel linked to radiation shields [4]. The cryostat can reach

T as low as 1.8 K by pumping on liquid ^{4}He. MLI are assembled on LN2 and LHe vessels. The sample chamber in LHe can be evacuated or filled with exchange gas for temperature variation. Sample cell and SC magnet are supported by S.S. tubes or G-10 rods with intermediate T thermal anchors.

A large vertical LHe II cryostat at CERN (Fig 2B) is developed for testing high field SC magnets [5]. The cryostat has a 3 m^3 LHe bath controlled between 4.2 K and 1.9 K. It can house magnets up to 2.5 m in length, 1.5 m in diameter, and 15 tons in mass. Cryogenic supply lines are permanently connected for faster insertion and removal. The cryostat has two LHe baths separated by a lambda plate, with saturated helium bath above and sub-cooled liquid helium bath below. The lower bath heat exchanger is filled with saturated liquid helium at 1.8 K. The magnet is supported by stainless steel plates and rods, with copper baffles. The neck of the cryostat has a heat intercept to limit conduction heat leak. The thermal shields (Cu) are actively cooled with helium gas and anchored with copper braids.

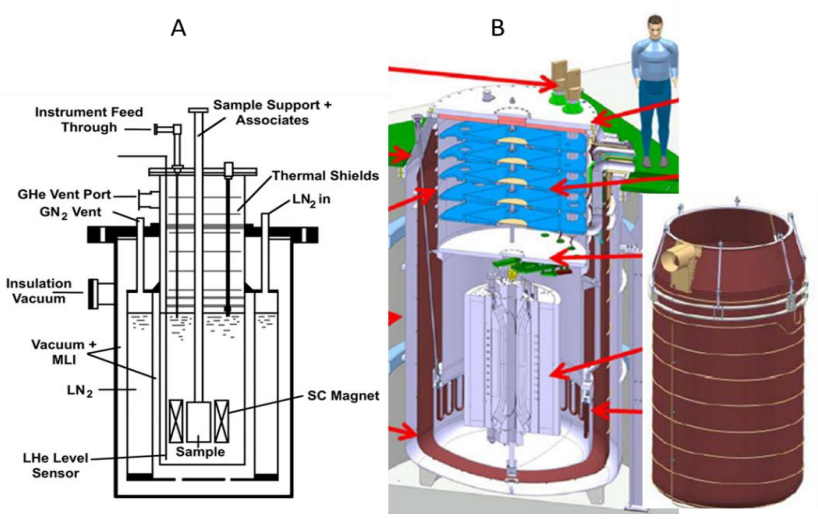

Figure 2. A: a Classic LHe cryostat [4]. B: large vertical LHe II Testing Cryostat [5].

2.2 Dry-Cryostat & Mixed Cooling Configurations

Dry cryostats are cooled by cryocoolers (such as G-M & Pulse tube cooler) without use of cryogenic liquid (Fig. 1B). The heat load of the sample/device is removed by a commercial two-stage cryocooler with thermal anchors (Cu or Al). One thermal anchor is connected between the first stage of the cryocooler and the thermal shield (40 - 80K), while the other is linked to the second stage and the sample (2 - 4K). These cryostats are compact and provide low operating costs, high autonomy, and flexible orientation. They require a high investment cost and may have vibration concerns.

The cryostat (Fig. 1C) is refrigerated using both cryogen and a cryocooler (as *Mixed-Cooling Cryostat)*. Typically, the first stage of the cryocooler is thermally anchored to the intermediate shields. The second stage is either thermally anchored to the re-condenser on top of the LHe-bath for recondensing vaporized He gas or connected to the LHe bath to greatly reduce boil-off. This closed-cycle cryostat is theoretically allowing for unlimited operation without additional liquid cryogen.

Anliker et al developed a cryostat for the SC undulator with several cryocoolers at 4.2 K for the SC undulator magnets and its LHe container (zero boil), 14-17 K for the beam chamber, and about 40 K for the thermal shield (Fig. 3A) [6]. The cryostat has three main components: a stainless-steel vacuum vessel, a thermal shield with 40 MLI layers, and a beam chamber. The cryostat also includes four turrets for mounting cryocoolers and instrumentation. As depicted in Fig 3B, Dhuley et al. utilized a Dry-cryostat configuration, where a 650 MHz single-cell elliptical Nb-Sn coated Nb cavity was coupled to a 4.2 K cryocooler through high-purity Al thermal links [7]. Without LHe, a Cryomech PT420 is used with 2 W at 4.2 K for the cavity and 55 W at 45 K for thermal shields. Conduction cooling near the cavity equator was chosen since the maximum RF heat-dissipations are concentrated in that area.

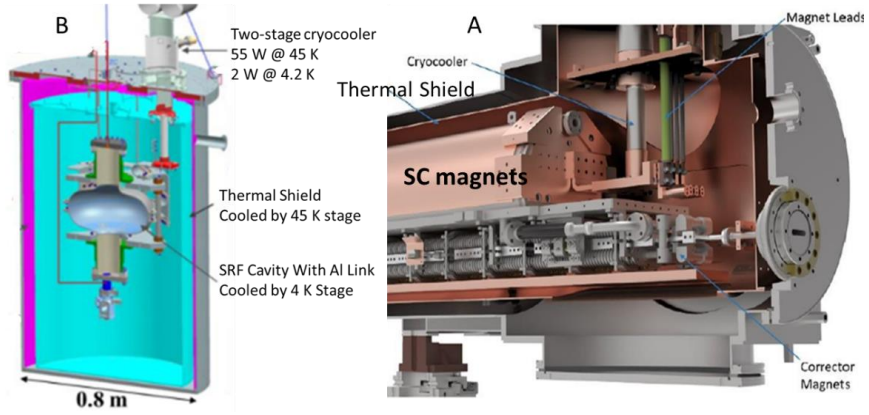

Figure 3. A: cryostat of SC undulator magnets [6]. B: dry cryostat of SRF cavity cooled only by a cryocooler [7].

The LHe II Bath Cryostat with Cryocooler Closed Loop as a *mixed-cooling method* eliminates the need for helium refill, offers advantages in efficiency and compactness. One example [8] of these successful creations is the cryostat with a He II liquefaction system for a 21-T magnet (with a warm bore for testing), where helium is cooled via a Joule-Thomson heat exchanger and enters the helium II heat exchanger as shown in Fig. 4. Helium vapor leaves the cryostat, is purified, and liquefied by a two-stage pulse tube cryocooler. Condensation can occur at the second-stage cold head.

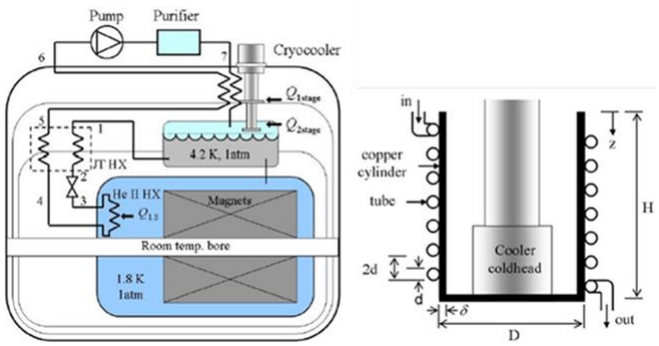

Figure 4. Schematic of cryostat with closed-loop cooling system for 21 T magnet and heat exchanger on extended surface of cryocooler [8].

2.3 Continuous Flow Cryostats

Originally, the cryostat (Fig. 1D) is *cooled by the continuing flows of LHe or LN2* from a Dewar. The sample temperature is controlled by adjusting the cryogen flow rate and using a heater in the loop. The operating time depends on the cryogen supply. Initially, they are commonly used for small samples in confined spaces, such as in various microscopes.

Since the 1980s, superconducting (SC) accelerators such as Tevatron, RICH, DESY, LHC have extensively used SC magnets and CEBAF, LEP, TESLA, XFEL, SNS and KEK have utilized large number of SRF cavities. Engineers and scientists have put significant effort into developing various cryostats to enable the success of these applications. Due to space limitations in this paper, we can only briefly illustrate a few representative examples to highlight their features.

The LHC (27-km accelerator) dipole magnet cryostat (13-m long and 1-m diameter) uses thermal shields to reduce heat loads from ambient to 2K temperature, with 30-40 MLI layers at ~65K and 10 MLI layers around ~1.9K cold mass [9]. The magnets are supported on low thermal conductivity posts and anchored at 50-65K and 6K (Fig 5A). Beam screens are crucial to minimize photo-desorbed gases and remove heat load. The new LHC project aims to increase proton collisions by a factor of ten and extend physics exploration until 2035. Challenges for the future cryostat design [10], as illustrated in Fig. 5B, involve integrating the cold mass, supports, thermal shield, and busbar lines within a 1-m-wide

cross-section. One of the constraints arises due to transport limitations in the LHC tunnel and cost consideration.

The TESLA (TeV Electron SC Linear Accelerator) Collaboration led by DESY Germany is an international R&D effort toward the development of an e^+e^- linear collider of 20 km [11]. TESLA stopped short due to financial reasons, but the core technologies achieved at TESLA have continuously advanced under many projects worldwide. Fig 5C shows a classic TESLA cryostat with 2K SRF cavity and high RF power input coupler, and Fig 5D is a SNS cryostat with the cavity and RF coupler [12].

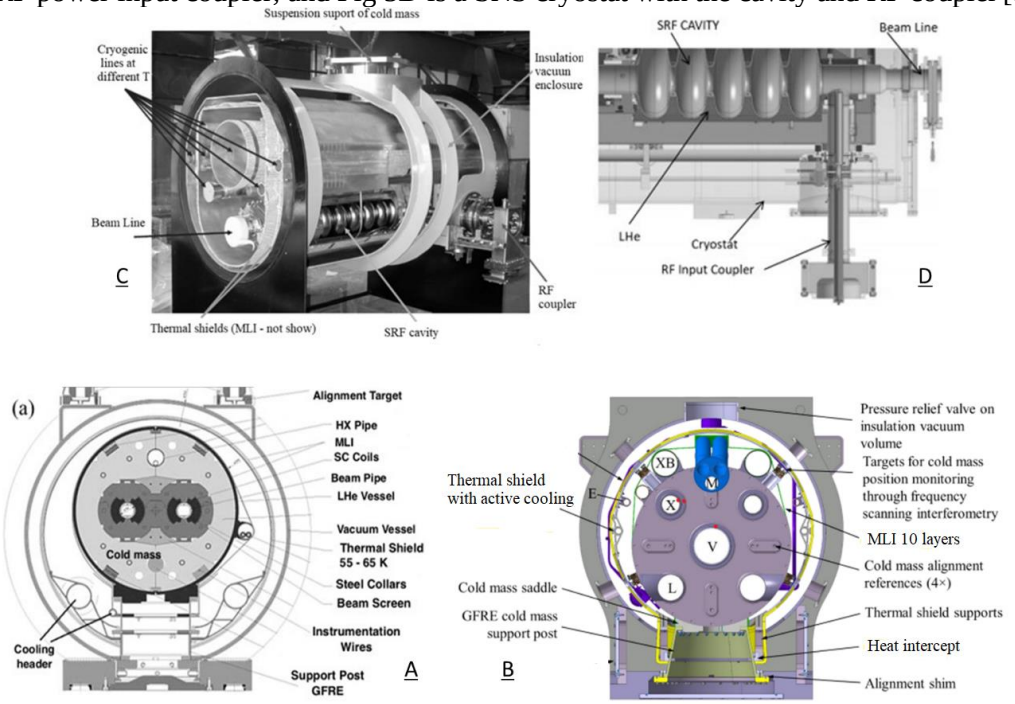

Figure 5. A: LHC magnet cryostat [9], B: cryostat for LHC future high luminosity magnets [10], C: cryostat for SRF cavity of TESLA/XFEL [11], and D: France SNS Cryostat [12].

2.4 Dilution Refrigeration Based Cryostats for below 0.3-K

Temperatures in the *cryostats below 0.3 K* are required in some special applications. *Dilution refrigerators (DR)* are used, which can reach as low as 2 mK (Fig. 1E). The cooling power is provided by mixing ^{3}He and ^{4}He isotopes. DRs have been utilized in modern physics, chemistry, material research and electronics. The need of larger mK cooling platforms for quantum computers is being driven by the desire to host ever growing numbers of cryogenic qubits in quantum computing platforms. As a leading effort, Fermilab's Colossus requires a large, cold space to build the world's largest dilution refrigerator (DR) for a SC quantum computer [13]. When Colossus is fully built, it will offer 5 cubic meters of cryogenic space and cool components to around 0.02K. That is about 10 times cooling power and 15 times volume than standard commercial dilution refrigerators. One of the unique features of the DR cryostat is that it has multiple thermal shields to minimize radiation heat from reaching the cold mass. As illustrated in Fig 6A, for the DR cryostat its vacuum shell is 3.4m diameter (D) 3.7m high (H). All other shields are first thermal shield 3m D – 2.8m H; He Shield 2.7m D, 2.6m H; 2K shield 2.5m D, 2.2m H; mix chamber shield 20m D, 1.5m H.

2.5 ADR-based Cryostats for Below Tens of mK

For temperatures lower than tens of mK, an *adiabatic demagnetization refrigerator (ADR)* is utilized in the cryostat (Fig. 1F). The basic operating principle of an ADR is to use a strong magnetic field to decrease the entropy of a material, producing refrigeration. Tuttle et al reported the development of a

space-flight ADR [14], which can provide continuous cooling at 50mK with more than 10 times the current flight ADR cooling power and reject the heat at 10 K and will also continuously cool a 4 K stage for instruments and optics (Fig 6B).

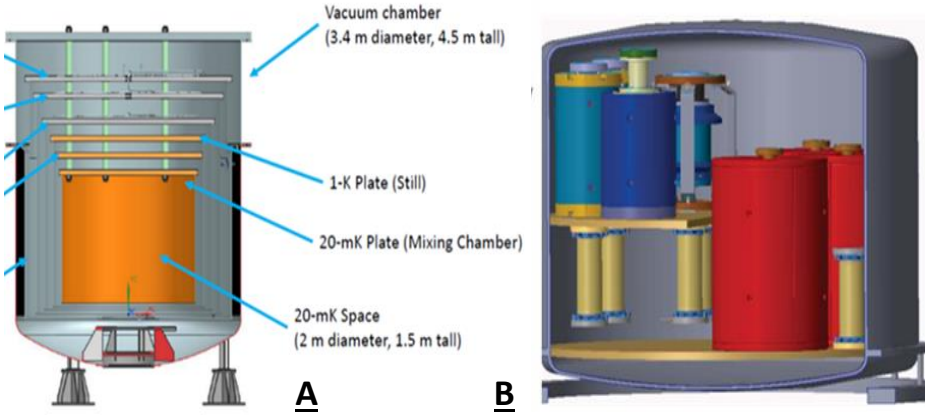

Figure 6. A, The world's largest dilution refrigerator of Fermilab Colossus for SC quantum computer [13]. B, The 4 to 0.05 K CADR (a space flight ADR) on the left inside a 35 cm (D) 10 K magnetic shield [14].

2.6 Special Cryostats for Space Missions

Cryostats for space missions are unique and face special challenges due to limited power, requiring very low heat leaks, lightweight, efficient/long-life cryocoolers, and the near-zero gravity. Strict thermal testing and quality control are necessary since repairs are often impossible in space. A key parameter is the signal-to-noise ratio (SNR), and the noise is proportional to T^3 (so low T is an essential requirement). Various cooling methods are used in space cryostats, including DR and ADR.

3. Design of Thermal Efficient, Light-Weight Support Structure

Supports in cryostats are critical components that serve multiple functions. They are designed to minimize heat flow through the support while providing adequate strength to withstand the cold-mass weight and impacts during transportation [15-16]. Depending on the specific requirements, they can be rigid (tension rods, pipes, support posts, rings, low thermal conductive discs), flexible (ropes, cables, straps, chains), or sophisticated structures with heat intercept stations [17-20]. Supports may need to allow for thermal contractions, sliding to accommodate thermal movements and specialized assembly requirements. Fig. 7 shows several advanced cryostat support systems and intermediate T stations have been incorporated into these support systems to minimize the heat load that reaches the cold mass [16].

3.1. Thermal & Mechanical Consideration of Support Materials

Suitable materials for cryogenic support must have low thermal conductivity and high mechanical strength/ductility. Examples of such materials include copper, nickel, copper-nickel alloys, aluminum and its alloys, austenitic stainless steels, titanium, and zirconium. Fiberglass composites like G-10/G-11 and Kevlar are also commonly used due to their strength, low thermal conductivity, and low outgassing. The ratio of strength to thermal conductivity, σ_y/k (N-K/W-m) is one important parameter to determine material suitability. Thermal conductivity integral $K = \int_{T_1}^{T2} k(T)dT$ and mean thermal conductivity $\bar{k} = \int_{T_C}^{T_H} k(T)dT\ /(T_H - T_C)$ are used to account for the non-linear changes in thermal conductivity with T. The heat transfer $\dot{Q}$ and cross section A (m^2) can be calculated as below, Where support length L (m).

$$\dot{Q} = \frac{\bar{k}_t A(T_H - T_C)}{L} \qquad A = \frac{F}{\sigma_a} = \frac{f_{safety}}{\sigma_y} F \quad (A \text{ for tension load})$$

Where F is the design load of the support member, where σ_a is the allowable stress for the support material, σ_y is the yield strength, and f_{safety} is the unitless factor of safety for the design. Representative values of $\bar{k}_t$ and σ_y/k for different materials can be found in the literature [16].

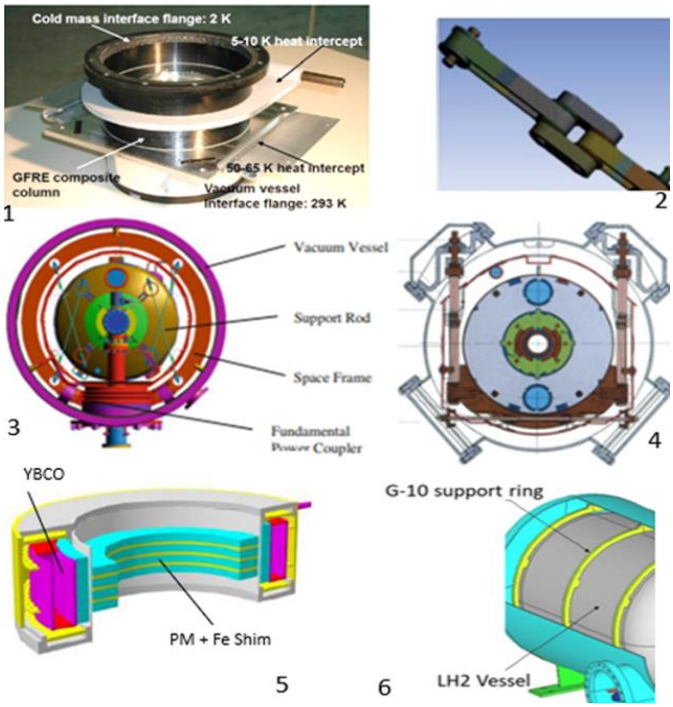

Figure 7. Sketches of cryostat support systems, which thermally isolate various cold masses from outer vessels at environment temperature [16]. 1, GFRE composite post. 2, Low thermal conductance strap/rope/cable. 3, support rods with ring combination. 4, Tension and compression rods (tubes). 5, HTS-PM Magnetic levitation support. 6, Ring with point contact support. Supports 1, 2, 3, 4 & 6 also have or able to have intermediate T heat stations.

3.2. Heat Interccept Stations at Intermediate T for Higher Efficient Support

Heat intercept stations at intermediate T at the cryogenic support are used to minimize the heat reaching the cold mass and reduce the refrigeration power required. The temperatures and distances of the stations along the support structure would be determined by the cooling sources available in practice and results by minimizing the Carnot refrigeration power [16]. For example, heat stations located along the uniform cross-section of a stainless-steel (or G-10) support, which may be in the form of a bar, tube, rope, or post. The total length of the support is L, which is broken into segments L_1, L_2, and L_3. The Carnot refrigeration power, P_{Carnot} is presented as the following:

$$P_{Carnot} = \eta_2 \dot{Q}_2 + \eta_3 \dot{Q}_3 + \eta_4 \dot{Q}_4 \qquad \text{where, Carnot efficient } \eta_i = \frac{T_1 - T_i}{T_i} = \frac{300 - T_i}{T_i}$$

The solutions show that the distance along the support at which a heat station is located depends on the temperature of the heat station. The Carnot power at the optimized locations for this support is provided in Fig. 8. The first stage or warm heat station was assumed to be at temperatures of 80 K, 70K, 65K, 55K and 45K. The refrigeration requirements can be minimized for the 4 K level with heat stations around 80 K and 20 K. When the T of the first station is lower, the T with minimum Carnot power at 2nd station is reduced. ANSYS & SINDA thermal analysis codes are utilized for sophisticated support systems.

4. Design & Optimization of MLI System

Currently, vacuum multilayer insulation (MLI) systems, also known as superinsulation, are widely used as the most efficient form of thermal insulation for cryostats in various applications. Demko, Fesmire & Shu have systematically introduced the theory, design, and performance data of MLI systems in a book by Taylor & Francis [21]. MLI systems consist of multiple radiation (or reflective) shields separated by low thermal conductivity spacers within an evacuated environment about 1×10^{-5} torr (Fig. 9). This design allows for effective thermal insulation by minimizing heat transfer through radiation and conduction. Typical reflector materials for example are 7-micron aluminum foil, single/double aluminized (~400 angstroms Al) Mylar, double gold coated Mylar and crinkled or microporous aluminized Mylar. Spacer

materials include micro-fiberglass paper (Lydall Cryotherm-243®, 25 microns thickness), polyester non-woven fabric, silk net, and discrete molded plastic spacers etc. There are many combinations of reflector and spacer with different number of layers, layer densities, and shapes of MLI blankets. Table 1 provides representative performance data of MLI systems from worldwide for convenient reference.

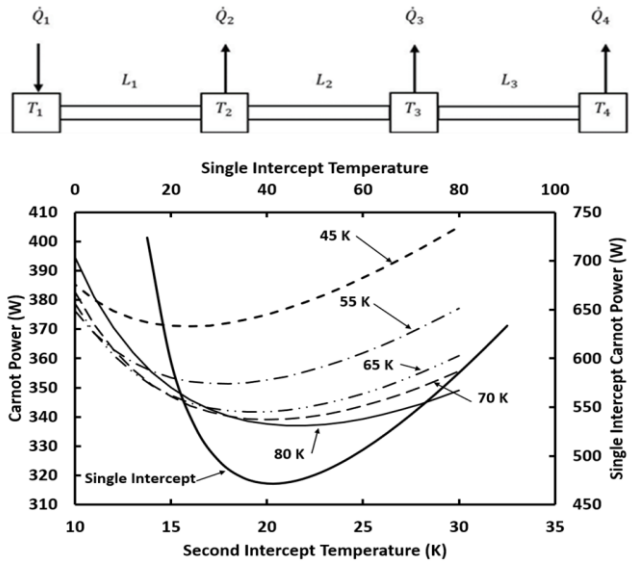

Figure 8. Upper: Uniform support between 330 K – 4K with two heat stations. Lower: A set of curves display calculated Carnot powers for different second heat station temperatures at optimal locations along the support, corresponding to varying temperatures offered by first heat stations. Generally for first heat station: LN2 provides 70-80 K, cold GHe 55-65 K, and cryocooler 45-55 K. Additionally, there is a curve illustrating the Carnot power vs single intercept temperature.

4.1. Selected Equations for MLI performance

Lockheed Equations [22]. The calculation models introduced here are based on data of MLI blanket tests from vertical cylindrical calorimeters. If silk net spacers and unperforated double-aluminized Mylar are use in the models, the coefficients are: Solid C_S = 8.95 x 10^{-8}, Radiation C_R, = 5.39 x 10^{-10}, and Gaseous C_G = 1.46 x 10^{-4}. (where, P - residual gas pressure, ε - effective emissivity).

$$q = \frac{C_s \times \overline{N}^{2.63}(T_h - T_c)\times(T_h + T_c)}{2\times(N+1)} + \frac{C_R \times \varepsilon \times (T_h^{4.67} - T_c^{4.67})}{N} + \frac{C_G \times P \times (T_h^{0.52} - T_c^{0.52})}{N}$$

Empirical Equation by CERN LHC. The equation for the MLI performance is developed for LHC SC accelerators. Modelling the thermal heat exchange through MLI can be complex. The simplified equation considers of two factors: radiation, which is a function of T^4, and residual solid conduction across the MLI blanket [23], Corrective factors β and α are to be determined experimentally.
T_1 – warm surface and T_2 -cold surface. For the LHC, the value β is 3.741 x 10^{-9} and α is 1.401 x 10^{-4}.

$$q = \frac{\beta}{N+1}\cdot(T_1^4 - T_2^4) + \frac{\alpha}{N+1}\cdot\frac{T_1+T_2}{2}\cdot(T_1 - T_2)$$

4.2. Intermediate T-shields for MLI System

The Carnot Efficiency represents the theoretical maximum efficiency of a cooling system, with Coefficient of Performance for cooling COPc = Qc/W_{in} = Tc/(Th-Tc), Qc is the heat removed, W_{in} is external work required. To remove the same amount of heat, the higher temperature level of the heat being removed, the lower the external works of the cooling device is needed. Therefore, using intermediate T shield is a crucial approach to improving thermal efficiency in real MLI systems (Fig. 9). Shu et al. introduced six representative cases [21,24] where shields were located between 300 K - 4 K and between 300 K - 20 K, and calculated the heat loads and minimum external work required. For example, in case 1, the heat from 300 K through 1 m^2 of 40 MLI layers reaching 4.2 K is 0.62 W, and it requires 43.6 W of refrigeration power to remove that heat. In case 3, there are 40 MLI layers on a 77 K shield and 20 MLI layers on a 20 K shield, resulting in a heat load of only 0.00064 W reaching 4 K. A total of 2.066 W of external work is needed to remove all heat [24].

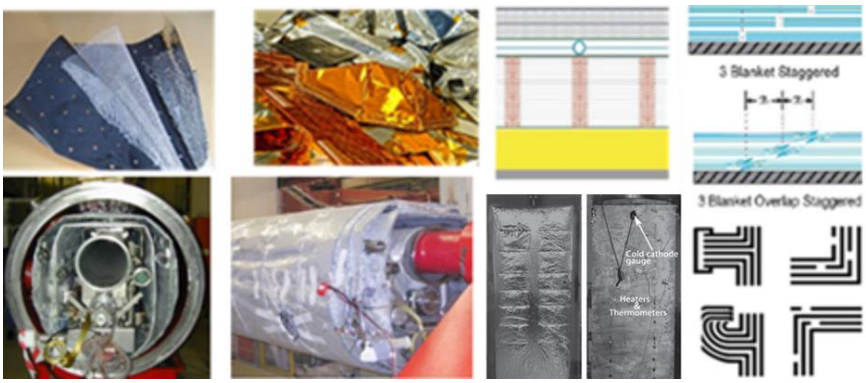

Figure 9. Left 4 Figs: Various MIL materials and MLI blankets on cold mass & thermal shield. Right 4 Figs: Testing of MLI blanket with crack/slot and practical designs of MLI blankets with/without cracks/seams.

4.3. Experimental Data of MLI Performance

Table 1 provides a selection of published results on MLI performance from various calorimeters developed for specific applications worldwide. However, the data may not be entirely consistent due to differences in MLI materials and workmanship used in different studies. Fig. 10 (left) [21] represents the typical performance of heat flux through the MLI blanket with a variation of layers from 0 to 90.

Table 1. Representative performance data of different MLI blankets at various (Th-Tc)

Authors	**Th-Tc K**	**Layers**	**Heat Flux W/m^2**	**Authors**	**Th-Tc K**	**Layers**	**Heat Flux W/m^2**
Fesmire [21]	293 - 78	40	0.39 - 0.59	Shu [21]	77 - 4.2	30	13.2x10^{-3}
Shu [21]	300 - 77	10 - 30	2.5 - 0.54	Ohmori [25]	64 - 5	20	25 - 34 x10^{-3}
Shu [21]	300 - 77	60 - 90	0.47 - 0.38	Nicol [26]	77 - 20	5 - 10	50 - 80 x10^{-3}
Ohmori [25]	298 - 70	50	1.5	Johnson [27]	260 - 19	30 - 50	~ 0.67
Mazzone [28]	300 - 80	10--30	2.5 - 0.5	Mazzone [28]	300 - 4	20 - 30	1.44 - 0.51

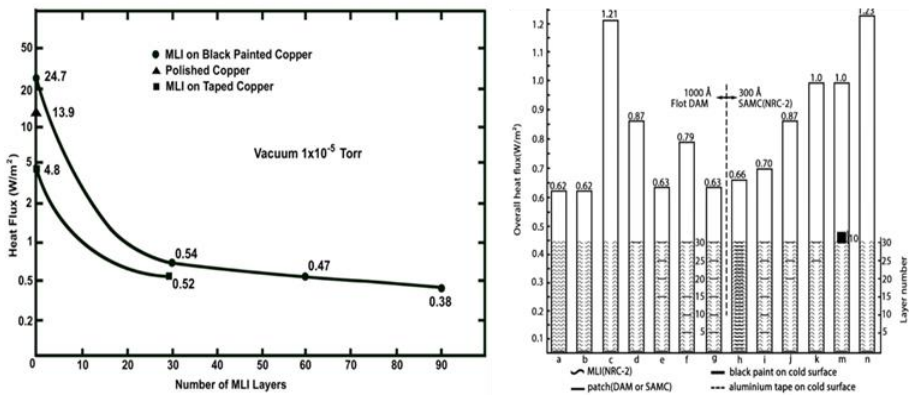

Figure 10. Left, Typical heat flux vs the number of MLI layers (on two cold surfaces). Right, height of column presents total heat to cold surface through MLI blanket in various cutting & patching.

4.4. Challenges and Solutions for MLI in Real-World Applications

MLI systems can experience compression and deformations due to weight and differential thermal contractions among shields, cold masses and supports during cooldown. Cracks, slots, and penetrations in real-world MLI systems can cause serious damages. An unexpectedly high heat flux of 117.5 W/m^2 was discovered through cracks in 300-77K experiments (and 221 mW/m^2 from 77-4K). Shu et al conducted experimental studies on the effects of cracks/slots on the heat loads through MLI blanks, proposing a theoretical model called "Enhanced Black Hole" to address this issue. Fig. 10 (right) presents a graphical summary of the "patch-cover-crack" experiments: A without cracks, B one-dimensional slits by sharp knife cuts, C & N without patches, and D to M different patch distributions [29]. Successful

resolutions have been developed by various investigators such as Johnson et al [21,27], creating several successful approaches to deal with cracks and seams in real applications, shown in Fig 9.

10. References

[1] Fesmire J, Shu Q-S, Demko J, 2022 Special Cryostats for Laboratory & Space Exploration (Chapter 12), Cryogenic heat management: technology & applications, CRC Press Taylor & Francis Group.
[2] Shu Q-S et al., 2015 Developments in advanced and energy saving thermal isolations for cryogenic applications, CEC/ICMC-2015
[3] Shu Q-S, 2007 Methodology of cryostat design, Tech Note, AMAC—TN 09M14, 2007.
[4] Shu Q-S, 2007 Methodology of cryostat design, Tech Note, AMAC—TN 09M15, 2007.
[5] Craena C, et al., 2014 New vertical cryostat for the high field superconducting magnet test station at CERN, AIP Conference Proceedings, 1573, 229 - [LL-10].
[6] Anliker E et al., 2020 A new superconducting undulator cryostat for the APS upgrade, IOP Conf. Series: Materials Science and Engineering, 755.
[7] Dhuley R et al, 2022 Development of a cryocooler conduction-cooled 650 MHz SRF cavity operating at ~10 MV/m cw accelerating gradient, IOP Conf. Ser.: Mater. Sci. Eng. 1240 012147
[8] Choi Y et al., 2008 Helium-liquefaction by a cryocooler in closed-loop cooling system for 21 T FT-ICR magnets, AIP Conference Proceedings, 985, 367.K
[9] Lebrun P, 2009 Cryogenics for particle accelerators, CAS Course, in General Accelerator Physics Divonne-les-Bains.K
[10] Ramos D et al., 2022 Final design of the cryostat for the high luminosity LHC magnets IOP Conf. Ser.: Mater. Sci. Eng. 1240 012136
[11] Carlo Pagani, ILC Cryomodule & Cryogenics, International Accelerator School for ILC, 2006 Japan.
[12] Howell M et al., 2015 Cryogenic system operational experience at SNS, IOP Conf. Series: Materials Science and Engineering, 101, 012127.
[13] Hollister M et al., A large millikelvin platform at Fermilab for quantum computing applications, IOP Conf. Ser.: Mater. Sci. Eng. 1241 012045
[14] Tuttle J et al, 2017 Development of a space-flight ADR providing continuous cooling at 50 mK with heat rejection at 10 K, IOP Conf. Series: Materials Science and Engineering, 278, 012009.
[15] Serio, L., Challenges for cryogenics at ITER, AIP Conference Proceedings 1218, pp. 651, 2010.
[16] Demko J, Shu Q-S, Fesmire J, 2022 Thermally Efficient Support Structures for Cryogenics (Chapter 4) Crypgenoc Heat management: Technology & Applications, CRC Press Taylor & Francis Group.
[17] Peterson T, 2017 Cryogenic Considerations for Cryomodule Design, at SLAC USPAS, 2017.
[18] Biallas G et al., 1987 The CEBAF SC accelerator cryomodule, IEEE. Magnetics MAG-23, Vol.2, 1987.
[19] Kaiser H, Design of Superconducting Dipole for HERA, DESY, Hamburg, Germany
[20] Shu Q-S et al.,2006 Magnetic levitation technology & exploration projects, Cryogenics, Vol. 46, No. 2–3.
[21] Fesmire J, Shu Q-S, Demko J, 2022 Multilayer Insulation Systems, (Chapter 3) Crypgenic Heat management: technology & Applications, CRC Press Taylor & Francis Group.
[22] Cunnington, G. et al., 1971. Thermal performance of multilayer insulations, interim report. LMSC-A903316/NASA CR-72605, Lockheed Missile and Space Company, Sunnyvale, CA.
[23] Parma, V., 2013. Cryostat Design, 2013 CERN School, Superconductors for Accelerators, May 2013.
[24] Shu QS, 2004 Private Tech Note, AMAC-TN-04-01, Virginia 2004.
[25] Ohmori, T. et al., 2014. Test apparatus utilizing Gifford–McMahon cryocooler to measure the thermal performance of MLI objectives background. ICEC 2014.
[26] Boroski, W., Nicol, T. et al., 1991. Design of the multilayer insulation system for the superconducting super collider 50mm dipole cryostat. ITSSC—1991.
[27] Johnson, W. et al., 2020. Performance of MLI seams between 293 K and 20 K. Advances in Cryogenic Engineering, IOP Conf. Series: Mater. Sci. Eng., 755 012152.
[28] Mazzone, L. et al., 2002. (MLI measurement) CERN LHC/2002–18 (ERC)
[29] Shu, Q.S. et al., 1987. A systematic study to reduce the effects of cracks in multilayer insulation, Part 1: Theory and Part II Experimental Studies. Cryogenics, Vol. 27, No. 298.

Acknowlegement

The authors express our sincere gratitude to our colleagues and the conference publishers for granting us permission to cite/use their published figures in the invited review paper.